doi.org/10.1002/cbdv.202300371 Research Article CHEMISTRY & BIODIVERSITY

www.cb.wiley.com

Isolation, Structure Elucidation and *in Vitro* Anticancer Activity of Phytochemical Constituents of *Goniothalamus wynaadensis* Bedd. and Identification of α-Tubulin as a Putative Molecular Target by *in Silico* Study

Akanksha Sharma[+],[a] Doddabasappa Talimarada[+],[a] Sundar N. Dhuri,[b] Venkata Narayanan Naranammalpuram Sundaram,[a] Duraippandi Palanimutu,[a] and Harish Holla*[a]

The phytochemical analysis of ethyl acetate and methanol extract of *Goniothalamus wynaadensis* Bedd. leaves led to an isolation of eight (**1**–**8**) known molecules, among them seven (**2**–**8**) isolated for the first time from this species, which includes (+)-goniothalamin oxide (**2**), goniodiol-7-monoacetate (**3**), goniodiol-8-monoacetate (**4**), goniodiol (**5**), (+)-8-epi-9-deoxygoniopypyrone (**6**) etc. The phytochemical modification by acetylation of **3** and **4** gave goniodiol diacetate (**9**) with absolute configuration (6*R*, 7*R*, 8*R*) confirmed by single crystal X-ray diffraction. Compounds **3**–**9** were cytotoxic against breast, ovarian, prostate and colon cancer cell lines with $IC_{50} < 10$ μM. Cell cycle analysis and Annexin-V assay on MDA-MB-231 cell using goniodiol-7-monoacetate (**3**) exhibited apoptotic response as well as necrotic response and showed cell proliferation arrest at G2/M phase. An *in silico* target identification for these molecules was carried out with an α-tubulin protein target by covalent docking. To gain an in-depth understanding and identify the stability of these protein-ligand complexes on thermodynamic energy levels, further assessment of the isolated molecules binding to the Cys-316 of α-tubulin was performed based on reaction energetic analysis via DFT studies which hinted the isolated molecules may be α-tubulin inhibitors similar to Pironetin. Molecular dynamics reiterated the observations.

Introduction

The Goniothalamus genus comes under the Annonaceae family and comprises about 160 species widely found in subtropical and tropical Asia regions.[1] Goniothalamus are rich in acetogenins, alkaloids, and styryl-lactone type of molecules.[2] Styryl lactones are found explicitly in the Annonaceae family and are one of the major phytoconstituents of Goniothalamus species apart from acetogenins.[3–7] These compounds are categorised primarily under the 5,6-dihydro-α-pyrones class of compounds found in plants, marine resources and microorganisms.[7] They possess α,β-unsaturated-δ-lactone ring skeleton with different substitutions at the C-6 position, as styryl (Ar–CH=CH_2), or substituted ethylbenzene (R–CHR′–CHR′′–Ar) type of substituents.[7] These α-pyrones are important pharmacophores responsible for the medicinal properties. α-Pyrones, with variable substitutions, have displayed a diverse range of biological activities, like anti-fungal, antimicrobial, antifeedant, anti-rheumatic, anti-osteoporotic, anticancer, etc.[2,7,8]

These styryl lactones having α-pyrone skeletons are not restricted to the Annonaceae family but are also spread in various plant families like Lamiaceae, Piperaceae, Lauraceae, Zingiberaceae, etc.[7,8] These types of secondary metabolites have been isolated from Cryptocarya, Polyalthia and Orthosiphon genera, which belong to one of these families. For example, phytochemical goniothalamin was initially isolated from *G. sesquipedalis* and was later found to be present in several other Goniothalamus species like *G. griffithi*, *G. malayanus*, *G. amuyon*, *G. gigantus*, etc.[2,5,10–12] Styryl lactone- Goniothalamin received the critical focus of research because of its therapeutic potential against various ailments like cancer, microbial infections, malaria, and osteoporosis, which has been continuously explored.[2,5,13–16] Other potent styryl-lactones isolated from this genus are 5-acetyl-goniothalamin, altholactone, isoaltholactone, 5-hydroxygoniothalamin and more.[2,6]

In the present study, a specific species of Goniothalamus was selected, *G. wynaadensis*, which is endemic mainly to Wayanad and Kannur regions, in Kerala and Kodagu region in Karnataka state, in India. From this species to date, only seven molecules have been reported, out of which four were lactones, namely goniopypyrone, goniothalamin, (+) altholactone, and 8-acetoxy-goniolactone.[17] Medicinal importance of the *G. wynaadensis* was reported among the tribes of Brahmagiri, Pushpagiri, and Nilgiri hilly regions of Wayanad, Mananthavady, Kerala, India, where they consume the bark juice of this species for the

[a] *Dr. A. Sharma,[+] Dr. D. Talimarada,[+] Dr. V. N. N. Sundaram, Dr. D. Palanimutu, Dr. H. Holla*
Department of Chemistry, Central University of Karnataka, Kalaburagi - 585367, India
E-mail: harishholla@cuk.ac.in

[b] *Prof. S. N. Dhuri*
School of Chemical Sciences, Goa University, Goa - 403206, India

[+] *Equal contribution.*

Supporting information for this article is available on the WWW under https://doi.org/10.1002/cbdv.202300371

© 2023 Wiley-VHCA AG, Zurich, Switzerland

joint related ailments.[18] Previously we have reported antimicrobial and anticancer analysis on the leaves extract of this plant species in different non-polar to polar solvents for the first time.[18] Based on our previously reported bio-guided fractionation, the more biologically potent ethyl acetate and methanol extracts were further subjected to the purification of individual phytochemicals in the present work. Apart from the goniothalamin and the synthesised compound, i.e., goniodiol diacetate, seven phytochemical molecules (**2**–**8**) were isolated for the first time from *G. wynaadensis* and one phytochemical molecule is synthesised in the present work. The isolated compounds were studied for the anticancer activity on four cancer cell lines visually ovarian (**SKOV3**), breast (**MDA-MB-231**), prostate (**PC3**) and colon (**HCT-15**) cancer cell lines. The tested set of compounds showed anti-proliferative potential with IC_{50} less than 10 μM for each. Cell cycle analysis on the selected molecules suggested the phases in which the compounds showed significant activity. Annexin V apoptotic assay further helped identify compounds with anti-apoptotic effects. Further, the *in silico* molecular modelling analysis and Molecular Dynamics (MD) simulation studies were performed to ascertain the molecular target for the plausible mode of action for compounds with the most potent anticancer activity.

Result and Discussion

Isolation and characterisation

The bio-guided fractionation of the leaves extracts of *Goniothalamus wynaadensis* displayed ethyl acetate and methanol extract to be active. Ethyl acetate extract (2.5 g) and methanol extract (2.0 g) was subjected to column chromatography using silica gel (60–120/100–200/230–400 mesh size) as stationary phase and eluted via gradient method using hexane-ethyl acetate as solvent. The pure compounds were isolated by multiple times running column chromatography and, at times, separated by RP-HPLC. The structures of isolated compounds were elucidated with the help of IR, 1D NMR (^{1}H-NMR, and ^{13}C-NMR), 2D NMR (COSY, HSQC, HMBC, and ROESY/NOESY), HR-ESI-MS and single-crystal X-ray diffraction (XRD) (*Supporting Information*). The obtained data for all the pure compounds were compared with the existing literature on different species of Goniothalamus, as well as from the species *Polyalthia parviflora*, to ascertain if the pure isolated compounds structures were reported earlier in these different species. The phytochemical analysis of AcOEt and MeOH extract led to the isolation of eight known phytochemical molecules, among them seven molecules reported for the first time from *Goniothalamus wynaadensis* Bedd. in this report (Figure 1).

The spectral data obtained for most of the isolated compounds have a common pattern: in the ^{1}H-NMR spectra, a broad multiplet signal at δ 7.2–7.4 for 5 Hydrogens hinted toward the presence of monosubstituted phenyl moiety (**1**–**8**) (Figure 1). The doublet signal varying near δ 6.0 and doublet of doublet signal varying at δ 6.9 was assigned to H3 and H4 of an α,β-unsaturated moiety, which may be part of δ-lactone ring in molecules (**1**–**5** and **8**), which was confirmed further by 2D NMR. Further, two different signals were observed for one proton each between δ 3–5 ascribable to H7 and H8 protons, which are deshielded due to heteroatom. The variation in the chemical shift for these two protons in all the compounds is

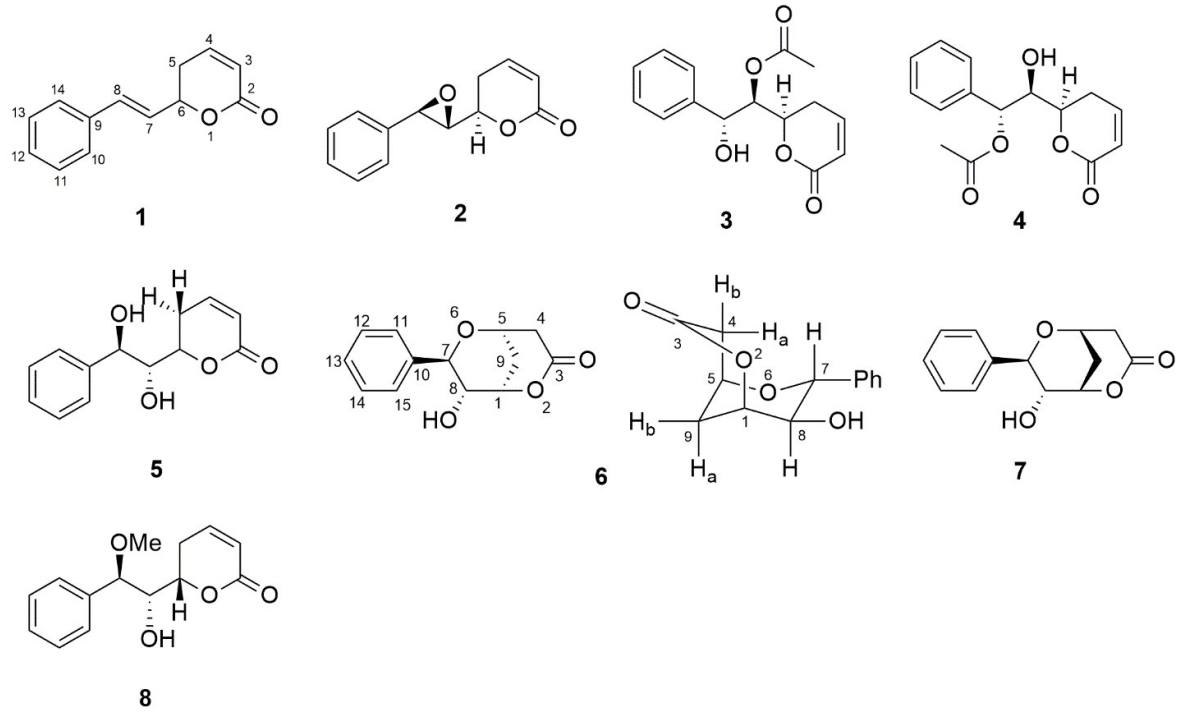

Figure 1. Compounds (**1**–**8**) isolated from the *Goniothalamus wynaadensis* Bedd.

© 2023 Wiley-VHCA AG, Zurich, Switzerland

due to the substitution of a different functional group, such as acetate, methoxy, alcohol and epoxide, at these carbon positions C7 and C8. These were also supported by ^{13}C-NMR spectra with observed signals between δ 60–80 ppm due to carbon attached to heteroatom oxygen.

Compound **1** was obtained as a solid with a melting point of 80–82 °C from the AcOEt fraction, and the ^{1}H–^{13}C-NMR data were similar to the reported compound goniothalamin (**1**). Its molecular formula was deduced to be $C_{13}H_{13}O_2$ based on its ESI-MS- *m/z* 201.2 $[M+H]^+$. This molecule was first reported from the bark of *Cryptocarya caloneura*;[19] later, the same molecule was also isolated for the first time by K. Jewers et al.[20] from the bark of *Goniothalamus andersonii*. This was also obtained from the *Goniothalamus wynaadensis* species.[17] Compound **2** was obtained as a viscous oil. The molecular formula was deduced to be $C_{13}H_{12}O_3$ based on its HR-ESI-MS- *m/z* 217.0862 $[M+H]^+$. The HR-ESI-MS data with *m/z* addition of 16 to goniothalamin (**1**) (ESI-MS- *m/z* 201.2 $[M+H]^+$) hinted at the addition of Oxygen atom possibly across the C–C double bond of goniothalamin (**1**). This observation was also supported by ^{1}H-NMR and ^{13}C-NMR data of compound **2**. Based on the ^{1}H-NMR and mass data, it was evident that the goniothalamin (**1**) was epoxidised at C7 and C8. The ^{1}H and ^{13}C-NMR spectra were found to be identical with the compound (+)-goniothalamin oxide (**2**), which was first time reported from *Goniothalamus macrophyllus* by Sam et al.,[21] and the absolute configuration of **2** was confirmed as 6*R*, 7*R*, 8*R* by Chuah et al.[22]

Compound **3** was obtained as a clear crystal solid with a melting point of 146–148 °C; the molecular formula was ascertained to be $C_{15}H_{16}O_5$ by HR-ESI-MS- *m/z* 277.1069 $[M+H]^+$. The ^{1}H and ^{13}C-NMR spectra resembled the unambiguous crystal compound, goniodiol-7-monoacetate (**3**), reported by Wu et al.[23] from the leaves of the *Goniothalamus amuyon*. Interestingly compound **3** and **5** isolation was first reported by Talapatra et al. in 1985[24] from the leaves of *Goniothalamus sespquipedalis* with relative configuration 6*S*, 7*S*, 8*S* based on Newman projections and steric repulsion arguments. However, later Wu et al. reported goniodiol-7-monoacetate (**3**) to have the absolute configuration as 6*R*, 7*R*, 8*R*[23] by single-crystal XRD and by circular dichroism (CD) studies. Further, a similar crystalline compound was obtained in the column chromatography, slightly polar to compound **3**, as a solid with a melting point of 112–114 °C. The molecular formula was confirmed to be $C_{15}H_{16}O_5$ by HR-ESI-MS- *m/z* 277.1071 $[M+H]^+$, which was

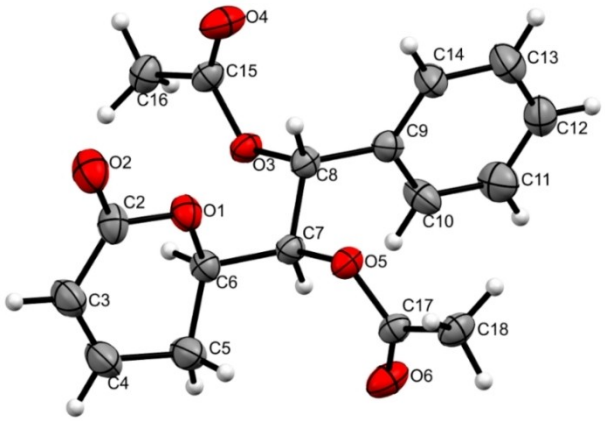

Figure 2. Crystal structure of compound **9**.

almost identical to compound **3**. However, there was a difference in the chemical shift value for H7 and H8 in the ^{1}H-NMR and a difference in the C7 and C8 value for the ^{13}C-NMR spectrum. Ironically the compound was found to be goniodiol-8-monoacetate (**4**), where the position of the acetate group was shifted to C-8 from C-7 in the case of goniodiol-7-monoacetate (**3**). This compound also was later found to be reported by Wu et al. in 1992[25] from the leaves of *Goniothalamus amuyon*. The relative configuration of the compound was reported as 6*R*, 7*R*, 8*R*.

In order to confirm the conflicting information on the relative configuration at C6, C7 and C8, we have attempted a simple acetylation reaction on compounds **3** and **4**. As compounds **3** and **4** only vary in the position of the secondary hydroxy group at C-8 and C-7, acetylation of these compounds was anticipated to yield the same product. So, compounds **3** and **4** were subjected individually to an acetylation reaction of the free hydroxy group (at C-8 in **3** and at C-7 in **4**, respectively), which delivered the same single-crystalline product goniodiol diacetate (**9**) (Scheme 1).

Further, compound **9** was subjected to crystal growth in a chloroform-ethanol medium by slow evaporation method and was subjected to single-crystal XRD (Figure 2), and the data has confirmed the compound (**9**) has an absolute configuration of 6*R*, 7*R*, 8*R* (*Supporting Information*). The melting point of compound **9** was found to be 155–157 °C which was identical

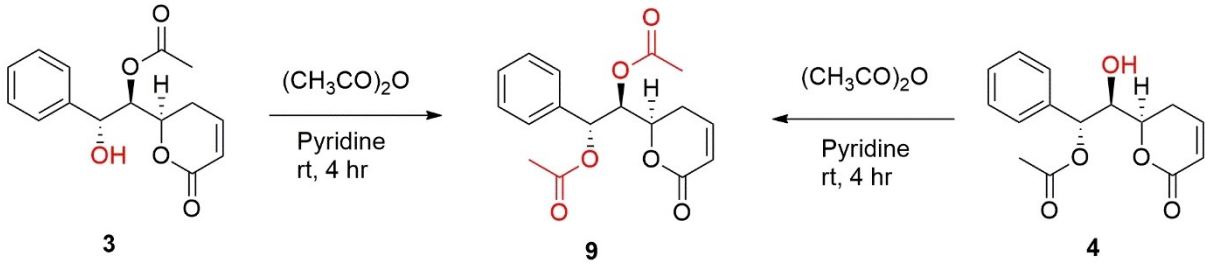

Scheme 1. Reagents and conditions: a) Goniodiol-7-monoacetate/Goniodiol-8-monoacetate (0.5 mmol) Pyridine (1 mmol), acetic anhydride (5 mmol), at room temperature, isolated yield about 85–90% 4 h.

© 2023 Wiley-VHCA AG, Zurich, Switzerland

to the earlier report, where the molecule was synthesised from the goniodiol-8-monoacetate by Wu et al.[25]

Compound **5** was obtained as a viscous oil; the molecular formula was deduced to be $C_{13}H_{14}O_4$ by HR-ESI-MS- at *m/z* 235.0966 $[M+H]^+$. The ^1H and ^{13}C-NMR spectrum data of this compound resembled goniodiol (**5**), which was earlier reported[24] from the leaves of *the Goniothalamus sesquipedalis* wall with relative configuration 6*S*, 7*S*, 8*S* at these stereogenic centers. This configuration was proposed based on a biogenetic pathway where goniothalamin (**1**) was expected to undergo epoxidation leading to (+)-goniothalamin oxide (**2**) followed by epoxide opening to produce goniodiol (**5**). However, later goniodiol (**5**) was reported by Fang et al.[26] with absolute configuration as 6*R*, 7*R*, 8*R*, which was further proven[27] by the supporting data of CD studies. Here, we have ascertained the structure based on extensive ^1H-^1H COSY, HMBC, HSQC and ROESY spectrum and by coupling constant values between H6, H7 and H8. Its specific rotation was found to be +38.70 (c = 0.0046, $CHCl_3$), which aligned to the absolute configuration of goniodiol (**5**) as 6*R*, 7*R*, 8*R*, as reported by Fang et al. earlier.[26]

Further, compounds **6** and **7** were purified from the polar fraction of ethyl acetate extract but required RP-HPLC. The linear gradient of methanol with water was used as the mobile phase in HPLC. Both compounds **6** and **7** were eluted at 40% of methanol with retention times of 16.54 min and 17.62 min, respectively. Compounds **6** and **7** were interesting and had puzzling spectroscopic features. Compound **6** was obtained as a white solid with a melting point of 130–132 °C, while compound **7** was slightly viscous. Compound **6** has displayed HR-ESI-MS at *m/z* 235.0965 $[M+H]^+$ and *m/z* 257.0782 $[M+Na]^+$, and compound **7** with HR-ESI-MS at *m/z* 235.0966 $[M+H]^+$ and *m/z* 257.0784 $[M+Na]^+$, which hinted at the probability of similar structural features with the possibility of diastereoisomer or enantiomer relation between **6** and **7**. Interestingly the molecular formula was the same as goniodiol (**5**), but NMR data has significant changes. In all the compounds **1** to **5**, the 5,6-dihydro-2-pyron ring, i.e., δ-lactone with conjugated unsaturation at C3 and C4, is present, but in the case of compounds **6** and **7**, H3, H4 and C3, C4 has moved to up field.

The 2D NMR data was of real significance here; the ^1H-^{13}C correlations by heteronuclear single quantum coherence (HSQC) spectrum of **6** exhibited the direct correlations between δ 2.99 [d, 1H (H-4a), 2.88 (d, H-4b)], and methylene proton signal at δ 2.23 (br. s, 2H (H-9)) to the methylene carbon signals at δ 36.5 (C4) and 29.8 (C9), respectively, confirming the presence of two methylene groups. The ^1H-^{13}C heteronuclear multiple bond correlation (HMBC) and ^1H–^1H correlation spectroscopy (COSY) spectra of **6** further confirmed the presence of two methylene groups and a saturated pyrone ring. The ^1H-NMR, ^{13}C-NMR and HSQC spectrum displayed the correlation of methine proton signals at δ 4.93, 4.46, 4.43 and 3.59 ppm to methine carbon signals at δ 76.7, 65.8, 74.3 and 72.6, which indicated the presence of four oxygen-bearing carbons of the probably fused pyrano-pyrone ring in **6**. The presence of one free-OH group was confirmed by the IR spectrum with hydroxy stretching at 3397 cm^{-1}. The overall data suggest that compound **6** has a phenyl pyrano-pyrone type skeleton.[22,28–31] Compound **6** has ^1H,^{13}C-NMR and 2D NMR parameters similar to (+)-8-epi-9-deoxygoniopypyrone (**6**), which have been reported earlier from the leaves of *Goniothalamus tamirensis*.[31] This structure was confirmed to have chair-boat conformation for fused pyrano pyrone skeleton, between the possible conformations of chair-boat, boat-boat and chair-chair conformation, which was confirmed by ^1H-^1H nuclear Overhauser effect spectroscopy (NOESY). The detailed explanation for the confirmation of chair-boat conformation present in the fused pyrano pyrone skeleton of compound **6** is described by Tai et al.[31] and Lan et al.[30]

Similarly, compound **7** was found to be mimicking compound **6** and was found to have a phenyl pyrano-pyrone skeleton. Comparison of the ^1H, ^{13}C-NMR and 2D NMR data of **7** with the available literature led to confirmation of the compound to be (−)-8-epi-9-deoxygoniopypyrone, which is an enantiomer of compound **6**. Compound **7** was previously isolated from the leaves of *Goniothalamus tamirensis*,[31] and the leaves of *Polyalthia parviflora*,[27] and the structure was unambiguously confirmed. It is straightforward that compound **6** and **7** is the product of intramolecular Oxa-Michael addition reaction on Goniodiol (**5**) in a suitable enzymatic condition in the plant species. All compounds **1**–**7** were separated from ethyl acetate extract.

The phytochemical investigation of the methanol extract (2g) also yielded the above compounds in minor quantities. It also yielded one more known compound, 8-methoxygoniodiol (**8**), previously isolated from the methanolic extract of *Polyalthia parviflora* leaves.[27] The compound **8** was obtained as a viscous oil; the molecular formula was deduced to be $C_{14}H_{17}O_4$ by HR-ESI-MS- at *m/z* 249.1118 $[M+H]^+$. The ^1H and ^{13}C-NMR data of this compound resembled goniodiol (**5**) with the methoxy group's replacement of the hydroxy group at C8. The presence of the methoxy group at C8 was confirmed by HMBC and ROESY spectrum (*Supporting Information*). The absolute configuration of the compound was reported and confirmed as 6*S*, 7*S*, 8*R*.

All the isolated molecules and synthesised compounds, except compounds **1** and **2**, were subjected to preliminary anticancer studies on four cancer cell lines which are tabulated below. Further, these molecules were run through *in silico* molecular modelling studies to find the possible target and pathway for the possible anticancer activity. Even though all the isolated molecules were reported earlier from different species of Goniothalamus, *Goniothalamus wynaadensis* Bedd. can be considered a single repository or storage tree for all these molecules in one species.

Preliminary anticancer activity

The test set of the molecules, along with the synthesised molecule **9** were subjected to preliminary MTT assay screening on four cancer cell lines ovarian (**SKOV3**), breast (**MDA-MB-231**), prostate (**PC3**) and colon (**HCT-15**) cancer cell lines and one normal cell lines. The MTT assay revealed that compounds **3**, **4**

© 2023 Wiley-VHCA AG, Zurich, Switzerland

and **8** displayed comparable cytotoxicity to vincristine in all four cancer cell lines tested (Table 1). The compound 8-Methoxygoniodiol (**8**) showed the most potent activity against ovarian cancer cell lines with IC_{50} 7.23 μM, better than standard vincristine. Goniodiol-7-monoacetate (**3**) and goniodiol-8-monoacetate (**4**) showed almost equivalent cytotoxicity against breast cancer cell lines at 7.49 μM and 8.06 μM, and goniodiol diacetate (**9**) showed slightly less potent activity in comparison with **3** and **4**. At the same time, removing the acetoxy group from both positions at C7 and C8 led to a significant reduction in cytotoxicity against MDA-MB-231 cells. This shows that the presence of acetoxy/methoxy group on the 7th or 8th carbon has a favourable effect on the cytotoxic effect of these compounds on breast cancer cell lines. The cytotoxic effects observed from the MTT assay represent these molecules as cytotoxic against SKOV3, MDA-MB-231, PC-3, and HCT-15 cancer cell lines but not against normal cell HEK-293, improving the therapeutic index.

Cell Cycle Analysis

To examine the effect of cell cycle progression, MDA-MB-231 cells were incubated with one of the potent isolated compounds, goniodiol-7-monoacetate (**3**) (HBT-96 A), at different concentrations (3,74, 7.49, 14.98 μM) for 24 h. Cells also were treated in the absence (untreated control) or presence of the positive control compound VIN (Vincristine). After staining the cell nuclei with PI (Propidium iodide), the percentage of cells at different phases of the cell cycle was quantified using flow cytometry (Figure 3 and 4). The treatment of the standard drug,

Table 1. Cytotoxic activity (MTT assay) of the isolated and synthesised compounds (**3**–**9**).

Compound	$IC_{50} \pm$ SD in μM (triplicate experimentation)				
	SKOV3	MDA-MB 237	PC-3	HCT-15	HEK-293
Goniodiol-7-monoacetate (**3**)	7.89 ± 2.02	**7.49 ± 1.38**	8.7 ± 0.78	8.51 ± 1.56	> 100
Goniodiol-8-monoacetate (**4**)	7.57 ± 1.09	8.06 ± 1.30	8.2 ± 1.26	8.89 ± 0.63	> 100
Goniodiol (**5**)	7.83 ± 1.58	> 100	8.0 ± 1.48	8.43 ± 0.49	> 100
(+)-8-Epi-9-deoxygoniopypyrone (**6**)	9.9 ± 1.02	8.45 ± 1.66	9.1 ± 1.20	8.06 ± 1.29	> 100
(−)-8-Epi-9-deoxygoniopypyrone (**7**)	> 100	7.67 ± 1.18	8.9 ± 0.67	8.10 ± 0.94	> 100
8-Methoxygoniodiol (**8**)	**7.23 ± 0.69**	10.72 ± 0.12	**6.7 ± 1.13**	**7.18 ± 1.88**	> 100
Goniodiol diacetate (**9**)	8.80 ± 1.89	9.79 ± 1.10	8.6 ± 0.96	8.84 ± 1.28	> 100
Vincristine	9.02 ± 1.28	7.00 ± 1.19	7.59 ± 1.33	6.14 ± 1.39	> 100

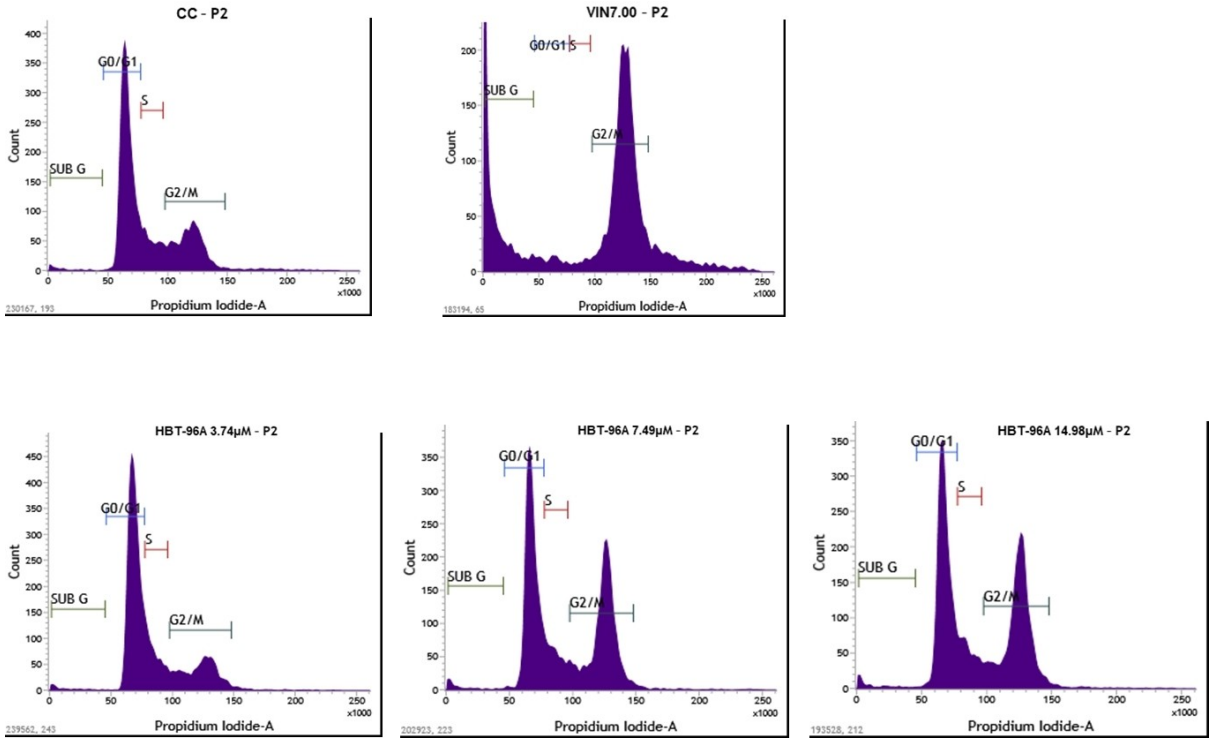

Figure 3. Flow-cytometric analysis on MDA-MB-231 cell lines; Vincristine and goniodiol-7-monoacetate (3) (HBT-96A) indicated concentrations. CC = Cell control, VIN = Vincristine.

© 2023 Wiley-VHCA AG, Zurich, Switzerland

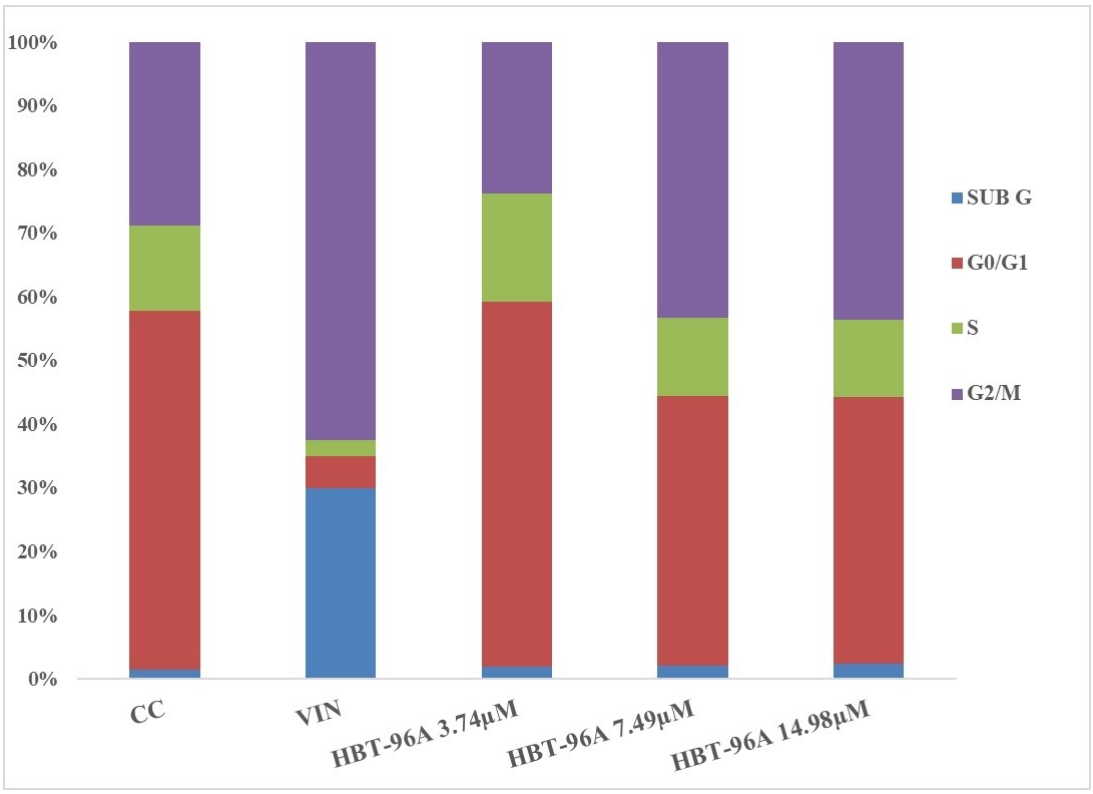

Figure 4. Flow-cytometry analysis on MDA-MB-231 cell lines: percentage of cell cycle arrest at different phases when treated with goniodiol-7-monoacetate (**3**) (HBT-96A) and vincristine.

vincristine (VIN), arrested the cell growth at the G2/M phase (53.66%) at its IC_{50} concentration (7.00 μM) along with a significant accumulation of apoptotic cell death at SubG1 (Figure 3 and 4) compared to untreated control. On the treatment of cells with HBT-96 A at its half IC_{50} concentration (3.74 μM), 55.57% cells were accumulated in G0/G1 phase and 23.12% cells in the G2/M phase which is almost similar to untreated control. However, when the concentration increased to its IC_{50} (7.49 μM), HBT-96 A caused a marked increase in the cell population at the G2/M phase (42%) with a concomitant decrease in the G0/G1 phase (41.01%) as compared to untreated control, clearly indicating G2/M phase arrest. Further increase in the concentration of HBT-96 A (14.98 μM) also caused G2/M phase arrest (42.3%) but not in a dose-dependent manner. At all three concentrations of the study, HBT-96 A cause no significant induction of apoptotic cell death at SubG1 relative to the untreated control. Cell cycle study clearly revealed that HBT-96 A arrested the cell growth in the G2/M phase at IC_{50} and higher concentrations with no significant accumulation of apoptotic cell death at SubG1.

Annexin V/ PI staining assay

Quantification of apoptosis was determined by using Annexin V/PI staining. MDA-MB-231 cells were treated with different concentrations of goniodiol-7-monoacetate (**3**) (HBT-96 A). This assay distinguishes the amount of live, early apoptotic, late apoptotic and necrotic cells, as shown in Figure 5. The results showed that goniodiol-7-monoacetate (**3**) increased the percentage of early apoptotic cells by 2.04% at 3.74 μM, 1.66% at 7.49 μM and 7.69% at 14.98 μM after 24 h treatment while the standard drug vincristine displayed early apoptotic cells by 11.80% at 7.00 μM. As shown in Figure 5a and b, on the treatment of compound **3**, the percentage of cells in the late apoptosis also increased compared to the control. The observed results suggest that the isolated compound, goniodiol-7-monoacetate (**3**), induced cell death through apoptosis in MDA-MB-231 cells. A significant percentage of necrosis is also observed but, in a dose, dependent manner.

In Silico target identification on isolated compounds

A molecular modelling study was performed to understand the role of the binding mode of the isolated molecules and their interactions. The docking study was performed on the molecules to analyse their interactions in an α-tubulin protein (PDB ID-5FNV) via Maestro, Schrödinger. Pironetin, an α,β-unsaturated δ-lactone isolated from Streptomyces species fermentation broths, is the only phytochemical known to bind α-tubulin. Pironetin has been reported as a potent cell cycle inhibitor which arrests cells in the M phase (IC_{50} in the range of 1.5–26 nM), and intravenous injection inhibits tumor growth in a

© 2023 Wiley-VHCA AG, Zurich, Switzerland

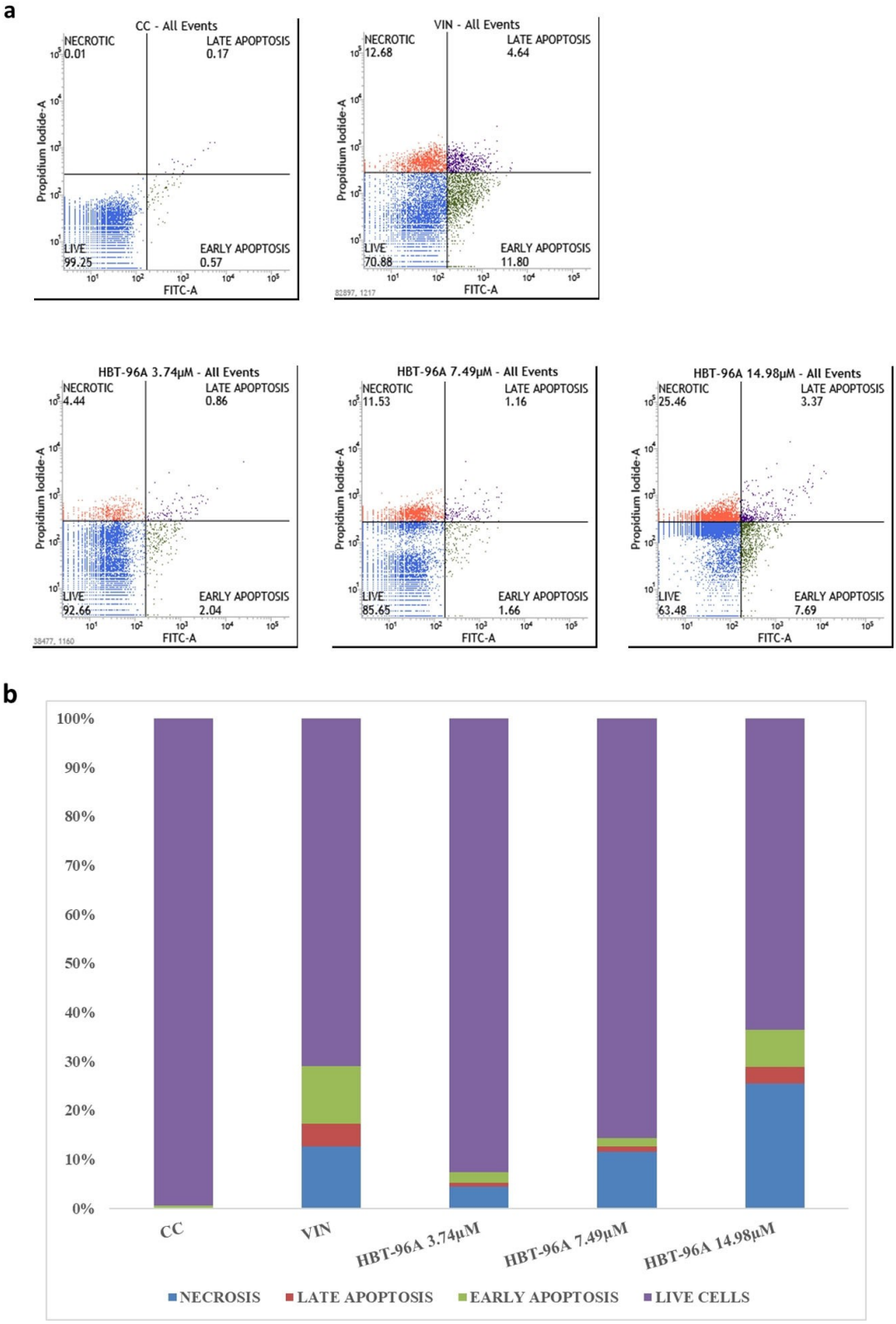

Figure 5. a) Flow cytometric analysis of apoptosis in MDA-MB-231 cells treated with goniodiol-7-monoacetate (**3**) (HBT-96A) and vincristine for 24 h. b) Percentage of cells in each phase represented in the bar graph.

mouse model of leukaemia at a dose of 6.3 mg kg^{-1}.[32–34] The isolated molecules from *Goniothalamus wynaadensis* Bedd. also have a common pharmacophore i.e., α,β-unsaturated δ-lactone in their structure. The α-tubulin-based tubulin polymerisation

© 2023 Wiley-VHCA AG, Zurich, Switzerland

inhibitor also has the same pharmacophore that is an α,β-unsaturated δ-lactone (Figure 1). In the present work, molecular docking studies were carried out on isolated lactone molecules against α-tubulin by covalent docking. Further, to support the molecular modelling, the energy and thermodynamic-based DFT analysis were also carried out via the Maestro Material Science Version 12.0.012 platform of Schrödinger software.

Tubulin protein crystal structures were obtained from the protein databank (PDB). The PDB id 5FNV was used in this study, and the Maestro Version 12.0.012 platform of Schrödinger software was used to process the three-dimensional structures of 5FNV protein and to locate the residue in the structure at 4 Å distance from the cysteine-316. The pharmacophoric similarity between the isolated compounds and pironetin, i.e., the presence of α,β-unsaturated δ-lactone ring, is one of the main justifications for choosing this protein structure. The α,β-unsaturated δ-lactone ring acts as a Michael acceptor and connects covalently to cysteine-316 in α-tubulin. This information intrigued us to choose α-tubulin as a target for molecular modelling and DFT studies. Protein preparation was done using the protein preparation wizard. Hydrogen atoms were added. Waters with less than three hydrogen bonds to non-waters were removed from the protein after sample water orientations were obtained using PROPKA at pH 7. Using the OPLS3e force field, the primary protease-ligand complex's restrained minimisation was accomplished. Finally, the protein was saved in PDB format for docking. Using the GetAccess (http://curie.utmb.edu/getarea.html)[35] software, the relative surface accessibility of the cysteine residues in the 3D structure of the α-tubulin protein was determined.

In a 2D sketcher of the Schrödinger software, the three-dimensional structures of the isolated molecules were created and saved with individual names, and the LigPrep panel was used to set up and start ligand preparation calculations. LigPrep was used to create stable low-energy 3D structures, which are then used to generate various protonation states, configuration, tautomers, and ring conformations for each input structure. Schrödinger software's Maestro Version 12.0.012 platform was used to perform the covalent docking analysis of α-tubulin with isolated molecules and determine the binding energy (kcal mol^{-1}). The receptor grid was defined in the coordinate region ranging from 10–12 Å by defining the amino acid residue at the active site of α-tubulin that is Cys-316 at chain C under default settings.

Very interestingly, the isolated molecules are binding in the same active site of the protein by the covalent binding at the Cys-316 residue of α-tubulin observed in, *in silico* studies. The observed interaction network of the isolated molecules with residues in the binding region is found to be similar to the reported results of docking of Pironetin (Figure 6a) at the active site of α-tubulin. We observed during molecular mechanics modelling studies via covalent docking method analysis study that the binding of compound **8** (Figure 6d) at the active site of the α-tubulin residues was comparable to that of standard α-tubulin inhibitor Pironetin. The docked pose of compound **8** on superimposition with Pironetin represented maximum alignment in line with the Pironetin binding pattern (Figure 6b). This seems to have an impact on the docking score of compound **8** with respect to Pironetin (Table 2). As per the studies reported, the Pironetin binding pattern to α-Tubulin is based on an induced fit mechanism.[36] The amino acid residues of α-tubulin on the Pironetin binding site undergo a major shift by 10 Å at the T7 loop and H8 helix (Cys-316, Leu-136, Phe-255, Leu-252, Leu-378). This, in turn, leads to the microtubule disassembly, as the resulting deviated but stable orientation of T7 loop appears to be attained in both α and β-subunits of Tubulin.[36] Hence, the isolated molecules specifically represented the stable interactions with Leu-136, Phe-255, Leu-252, and Leu-378.

Table 2. Docking score of test set compounds and standard compounds.

Sl. No.	Comp.	Docking score	Amino acids involved in different interactions			
			Covalent bonding interaction	Hydrogen bonding interactions	Polar interactions	Hydrophobic interaction
01	Pironetin	−7.325	CYS-316	ILE-238	GLN-256, SER-165, GLN-133, SER-241, THR-239, SER-241	LEU-378, MET-377, CYS-376, LEU-318, LEU-317, CYS-316, VAL-353, PHE-202, PHE-255, LEU-167, CYS-4, LEU-252, PHE-135, LEU-136, LEU-242, LEU-248, GLY-354
02	**1**	−6.491	CYS-316	SER-241	SER-165, GLN-256, THR-239, GLN-133,	LEU-242, LEU-378, ILE-238, PHE-202, CYS-4, LEU-136, LEU-167, PHE-255, LEU-259, LEU-252
03	**2**	−7.093	CYS-316	SER-241	THR-239, GLN-256, GLN-133, SER-165	LEU-259, LEU-242, LEU-378, ILE-238, PHE-202, LEU-136, LEU-167, LEU-252, CYS-4, PHE-255
04	**3**	−7.25	CYS-316	ILE-238	GLN-256, SER-241, THR-239	PHE-255, LEU-318, LEU-378, LEU-252, LEU-136, LEU-167, LEU-242, ILE-238, PHE-202, CVY-200, LEU-259
05	**4**	−7.064	CYS-316	ILE-238	THR-239, SER-241, GLN-256	LEU-318, LEU-378, LEU-259, PHE-202, PHE-255, CYS-200, LEU-167, LEU-136, LEU-252, CYS-4, LEU-242
06	**5**	−7.201	CYS-316	SER-241, ILE-238	THR-239, SER-165, GLN-256	LEU-259, LEU-378, PHE-202, PHE-255, CYS-4, LEU-136, LEU-252, LEU-167, LEU-242
07	**8**	−7.979	CYS-316	ASN-258, ILE-238	SER-241, THR-239, GLN-256	LEU-256, PHE-202, LEU-167, PHE-255, LEU-136, LEU-259, LEU-242, LEU-318, LEU-378
08	**9**	−6.752	CYS-316	–	SER-237, THR-239, SER-241, GLN-256	LEU-318, LEU-378, VAL-260, LEU-259, PHE-202, PRO-268, LEU-167, CYS-200, PHE-255, CYS-4, LEU-136, LEU-252, LEU-242, LEU-248, LEU-238

© 2023 Wiley-VHCA AG, Zurich, Switzerland

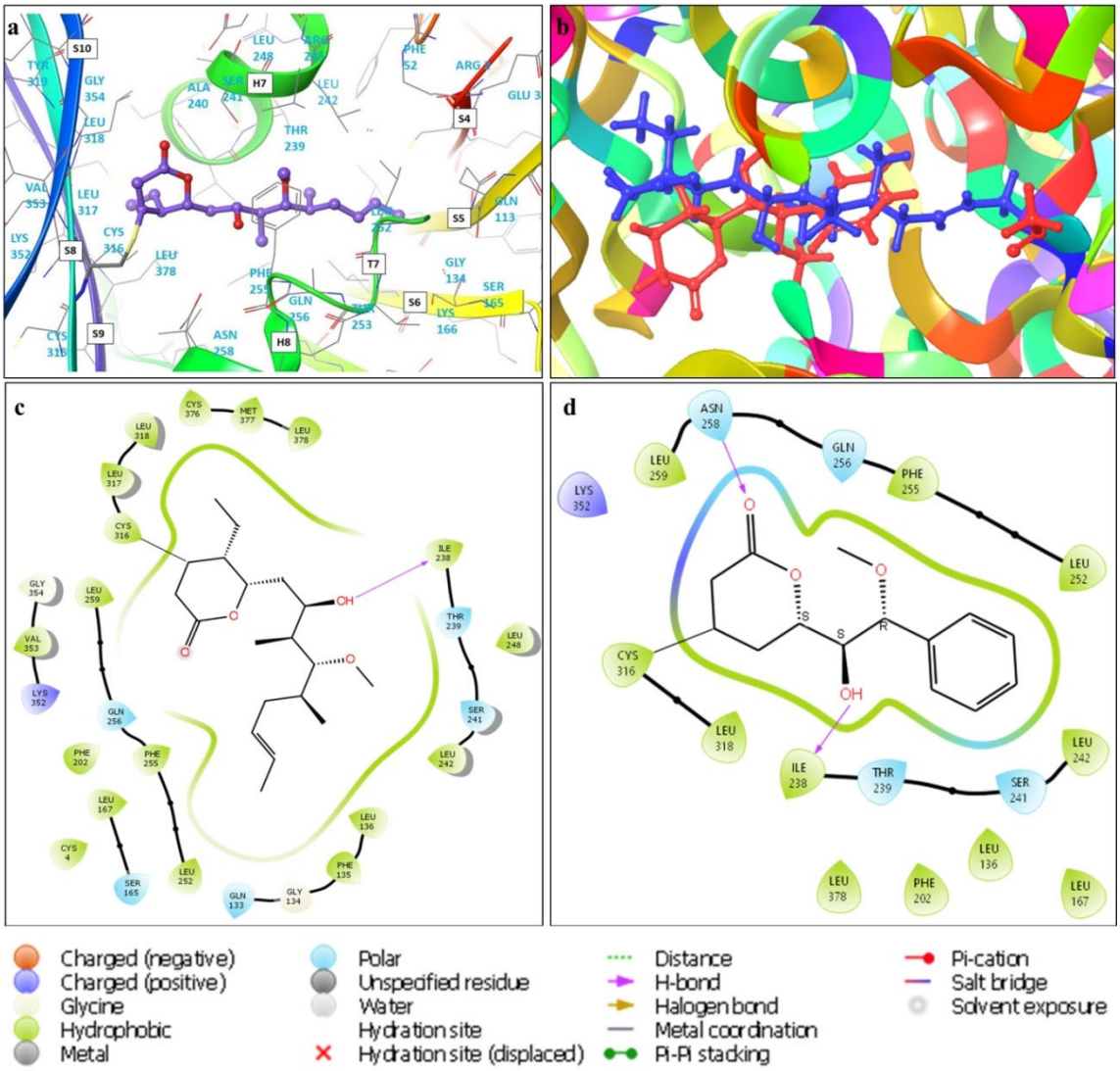

Figure 6. a) The molecular docking image (3D) of compound Pironetin in complex with α-tubulin and its interactions with amino acid residues. b) Display of relative positions and interactions of 8-methoxygoniodiol (**8**) with Pironetin towards the α-tubulin complex. c) Major interactions of amino acids residue within 4 Å regions at the α-tubulin binding site to 8-methoxygoniodiol (**8**) and d) Major interactions of amino acids residue within 4 Å region at the α-tubulin binding site to standard ligand Pironetin.

Compound **8** with maximum alignment showed slightly higher docking scores (Table 2) during docking analysis than Pironetin.

Computational study of the reaction between cysteine thiol group and isolated molecules

To gain an in-depth understanding and identify the stability of these protein-ligand complexes on thermodynamic energy levels, further assessment of the isolated molecules binding to the Cys-316 of α-tubulin was performed based on reaction energetic analysis via DFT studies. To understand the mechanism of formation of covalent bonding between isolated molecules and Cys-316 in the protein α-tubulin, 2D structures of isolated molecules and Cysteine were sketched and imported into the 3D workspace, which was followed by minimisation and optimisation. Molecules were optimised using B3LYP–D3 on the Jaguar platform (version: 10.2, Schrodinger release 2019-2) with a 6-31 G** basis set and polarisation function on all atoms. The accuracy level was set to ultrafine and maximum iteration steps of 100 with a switch to analytical integrals near convergence. The optimised molecules were imported into the Jaguar reaction module to calculate Gibbs free energy (Scheme 2). Gibbs free energy change (△G) values for putative reactions between Cysteine and isolated molecules were calculated by density functional theory (DFT) on the Maestro Material Science 3.4.012 platform of Schrodinger software. Gibbs free energies are stated in (kcal/mol) assuming standard condition (T = 298.15 K and p = 1.0 bar). HOMO and LUMO structures of the molecules were also obtained along with the optimisation (supplementary information). The possible Michael addition reactions of Cys-316 with isolated molecules

© 2023 Wiley-VHCA AG, Zurich, Switzerland

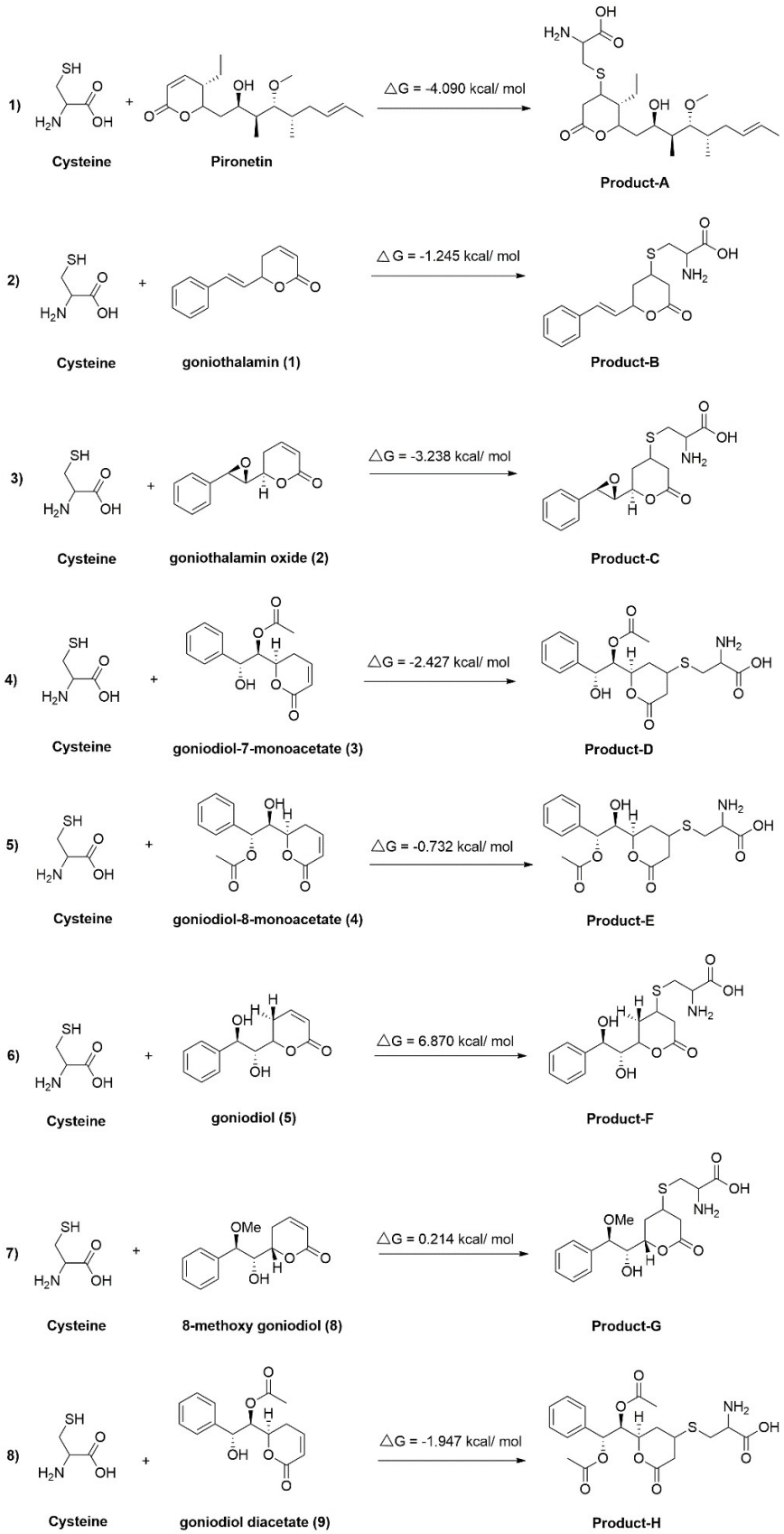

Scheme 2. A computational study for the probable reaction of Cysteine with isolated molecules (change in free energy – △G values in kcal/mol).

© 2023 Wiley-VHCA AG, Zurich, Switzerland

(Scheme 2) were carried out using the Schrodinger Material Science suit.

The results suggest that nucleophilic attack by cysteine thiol on an α,β-unsaturated δ-lactone results in the formation of a new covalent bond. The Gibbs free energy change for the reaction of cysteine thiol with Pironetin is found to be −4.090 kcal/mol (Scheme 2). This indicates that the reaction is spontaneous and, in turn, suggests that there is no need for additional energy to facilitate the occurrence of the reaction in the form of input energy or through the stabilisation of the products, and interestingly Yang et al. group presented similar results experimentally.[37] In the present study, the isolated molecules undergo a Michael addition type reaction with Cysteine thiol in an α-tubulin protein. The values of Gibbs free energy change for the isolated molecules are shown (Scheme 2), which indicates that the reactions are spontaneous and they have a good affinity to undergo Michael addition reaction. When we compare the results of docking score and △G values by DFT, all the isolated molecules show comparable scoring function with respect to Pironetin and negative △G values, i.e., spontaneous reaction except for goniodiol (**5**) and 8-methoxygoniodiol (**8**) where it is thermodynamically unfavourable and displayed positive △G values. Hence, the DFT analysed nucleophilic attack on isolated molecules indicates that these molecules can act as an inhibitor of α-tubulin.

Molecular Simulation Studies

As per the *in vitro* studies, 8-methoxygoniodiol (**8**), and goniodiol-7-monoacetate (**3**) were observed to be the most potent compounds. The biological results (Figure 4 & 5) seemingly correlated with the covalent molecular docking analysis (Figure 6 & 7) with α-tubulin as well as the Michael addition between cysteine thiol with α,β-unsaturated δ-lactone represented stability potential during the DFT analysis. Thus, molecular dynamics simulation studies were performed to confirm the stability of predicted docked poses interactions and understand the nature of molecular interactions. A total range of 19,595–19,598 water molecules were kept in the complex simulation box. The system simulation captured 1000 structures from the trajectory during a runtime of 100 nanoseconds. The RMS deviations of each protein-ligand complex, 8-methoxygoniodiol (**8**) (Figure 8), and goniodiol-7-monoacetate (**3**) (Figure 9) structures with α-tubulin obtained from MD simulation were plotted.

8-Methoxygoniodiol (8)

The protein backbone, C-alpha chain, represented a well-stabilised interaction from 30 nanoseconds (nsec) frame onwards. The protein-ligand fitting complex during the MD simulation run showed a maximum storm displacement between 1.3–1.4 Å in the 30–100 nsec run within the acceptable range of 2 Å. The RMSF plot **(Figure 8b)** further displayed the least fluctuations and stability of the ligand-protein complex binding with amino acid residues. The majority of interactions in the protein-ligand complex were Hydrogen bond (H-bond), hydrophobic and via water bridges with respective amino acid residues, as observed from the Histogram plot **(Figure 8c)**. Among these, H-bonding with ILE-238, ASN-258, SER-241 and hydrophobic connectivities with LEU 242, PHE-202 and the hydrophobic connectivities accompanied by water bridges and

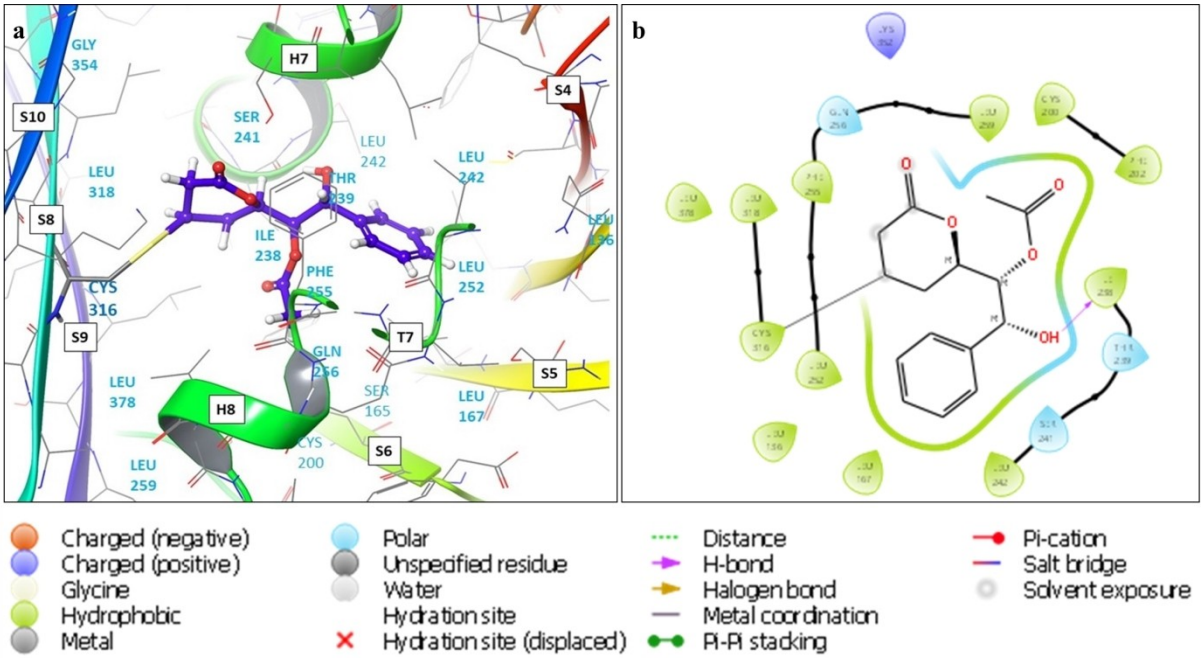

Figure 7. a) The molecular docking image (3D) of compound goniodiol-7-monoacetate in complex with α-tubulin and its interactions with amino acid residues. b) Major interactions of amino acids residue within 4 Å regions at the α-tubulin binding site to goniodiol-7-monoacetate (**3**).

© 2023 Wiley-VHCA AG, Zurich, Switzerland

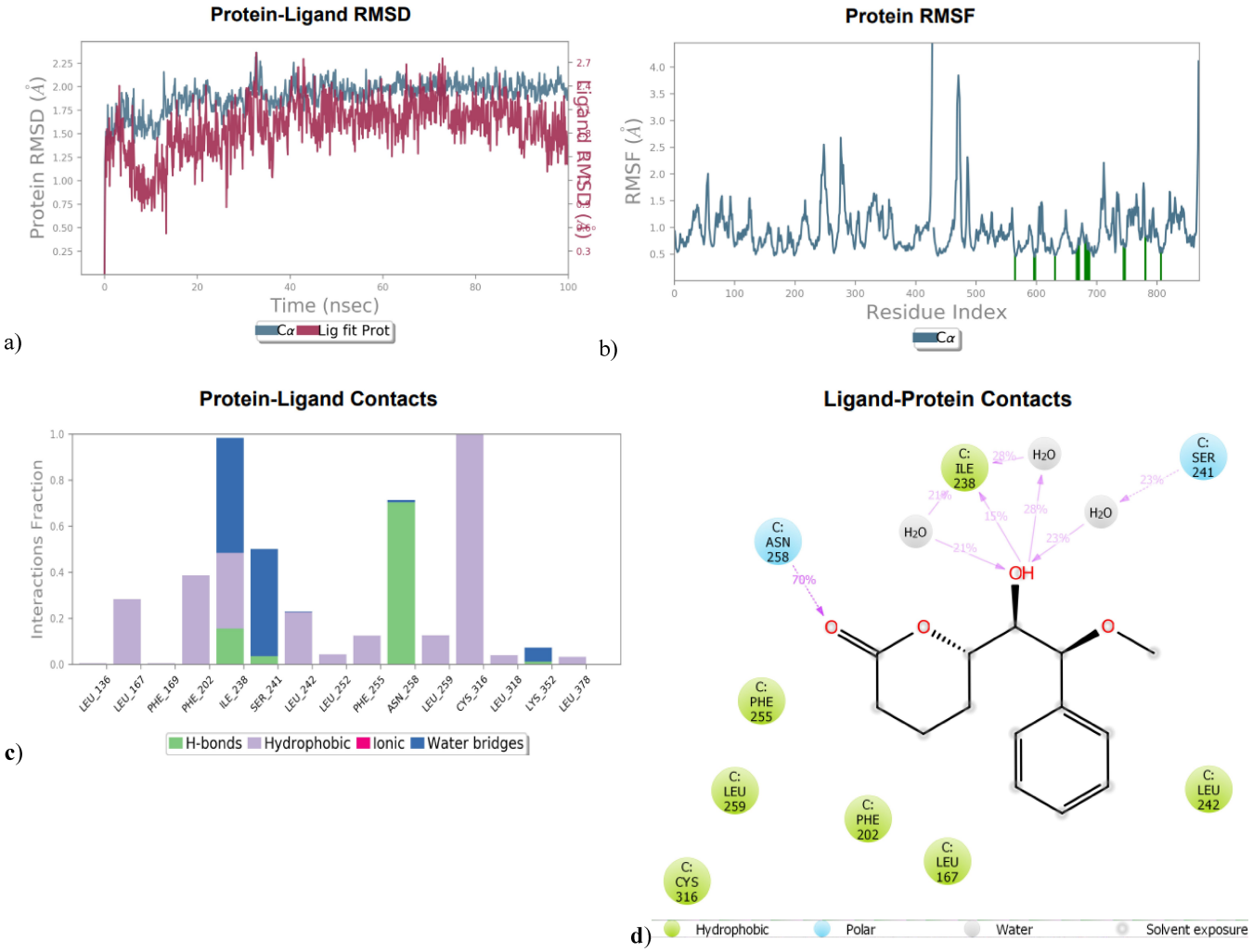

Figure 8. a) Compound 8 Protein-ligand RMSD plot; b) Protein-ligand RMSF plot; c) Histogram plot of compound 8; d) Protein-ligand complex with crucial amino acid residues in interaction.

H-bonding for ILE-238 are all crucial interactions at the active binding pocket of the protein that was maintained during the majority time fraction of the MD Simulation period.

Goniodiol-7-monoacetate (3)

The MD simulation run suggested that Goniodiol-7-monoacetate formed a stable complex with C-alpha chain of the protein. The stability of the complex could be observed from 20 nsec onwards in the protein-ligand fitting RMSD plot (Figure 9a). RMSD between 20–100 nsec ranged from 1–1.4 Å, well within the permitted range of RMSD. The RMSF plot (Figure 9b) representing ligand connectivities displayed minuscule fluctuations with the active pocket binding amino acid residues. Most of the ligand's interactions are hydrophobic and H-bonding based and were maintained for the most time during the MD simulation run, which is more than 30% of the time frame as per the histogram plot (Figure 9c). Connectivities with LEU-259, PHE-255, LEU-242, SER-241, and ILE-238 were the major interaction between amino acid residues and ligands.

Conclusions

The phytochemical analysis of ethyl acetate and methanol extract of *Goniothalamus wynaadensis* Bedd. leaves led to the isolation of eight (**1**–**8**) known molecules; seven (**2**–**8**) molecules were isolated for the first time from this species. The phytochemical modification by acetylation of **3** and **4** gave goniodiol diacetate (**9**) with absolute configuration (6*R*, 7*R*, 8*R*). Compounds **3**–**9** were selectively potent against MDA-MB-231, SKOV3, PC-3 and HCT-15 cell lines with $IC_{50} < 10$ μM. Cell cycle analysis and Annexin-V assay on MDA-MB-231 cell using goniodiol-7-monoacetate (**3**) exhibited apoptotic response as well as necrotic response and showed cell proliferation arrest at G2/M phase.

Further, an *in silico* target identification for the isolated molecules was carried out with an α-tubulin protein target by

© 2023 Wiley-VHCA AG, Zurich, Switzerland

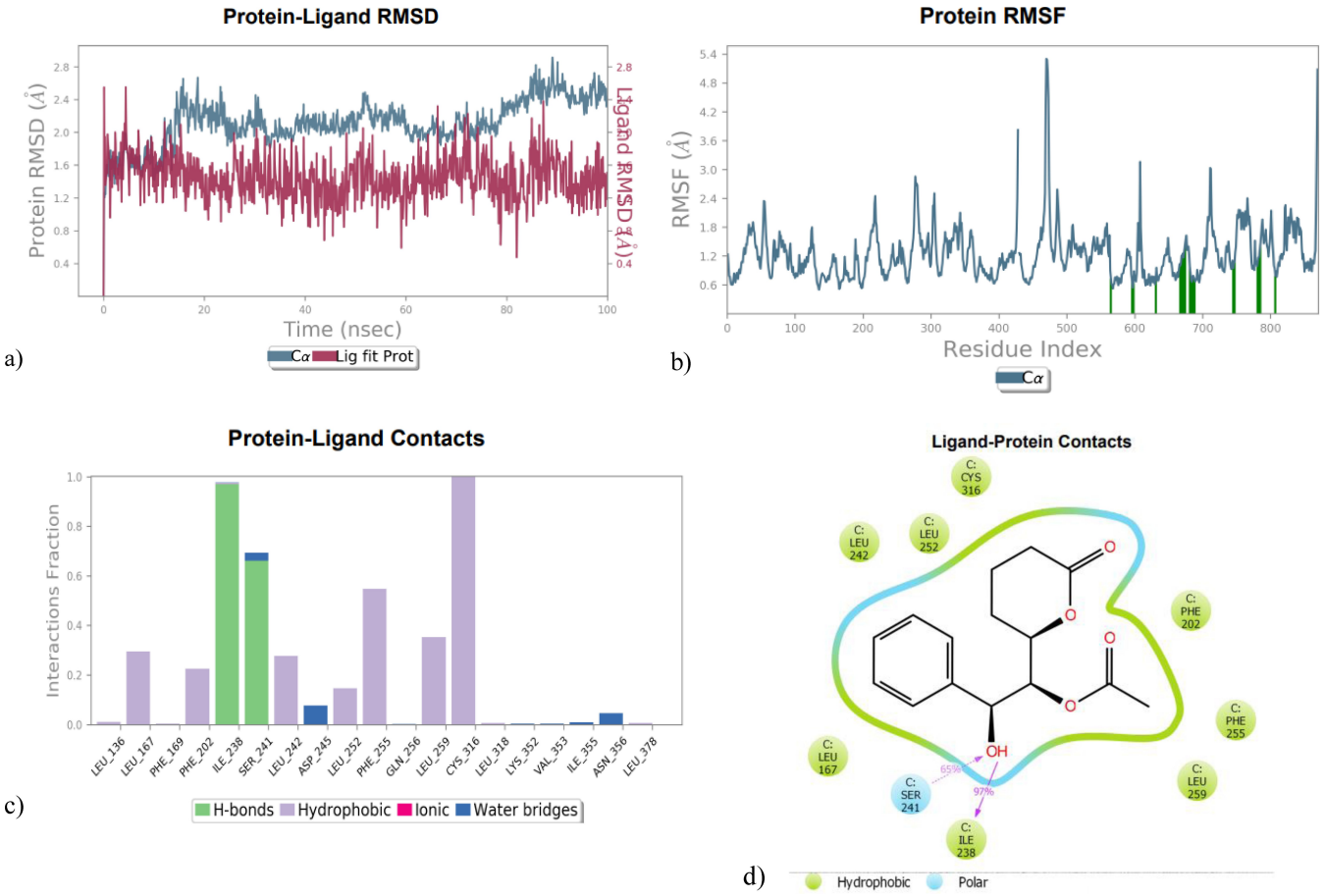

Figure 9. a) Compound **3** Protein-ligand RMSD plot; b) Protein-ligand RMSF plot; c) Histogram plot of compound **3**; d) Protein-ligand complex with crucial amino acid residues in interaction.

covalent docking. Compound **3** and **8** displayed docking score of −7.25 and −7.979 comparable to α-tubulin inhibitor, Pironetin, at −7.325. To gain an in-depth understanding and identify the stability of these protein-ligand complexes on thermodynamic energy levels, further assessment of the isolated compounds binding to the Cys-316 of α-tubulin was performed based on reaction energetic analysis via DFT studies, which hinted the isolated compounds may inhibit α-tubulin, similar to Pironetin. Molecular dynamics simulation performed on compound **3** and **8** in the binding pocket of α-tubulin confirmed the stability of predicted docked poses interactions and reiterated the nature of molecular interactions in the binding site. We can conclude here that the isolated new molecules are potential anticancer compounds, and more different chemical modifications can be carried out with the inputs from *in silico* studies to develop a promising anticancer candidate.

Experimental Section

General experimental procedures

IR spectroscopic data were obtained via Perkin Elmer spectrum II FT-IR. High-resolution mass spectra (HR-MS) were obtained on an FTMS in ESI mode. NMR 1D and 2D NMR were performed with Bruker Avance 500 and 400 MHz, with TMS being the internal reference. Column chromatography (CC) for isolation of secondary metabolites was carried out with Merck-Sigma Aldrich silica gel of mesh size 60–120, 100–200, and 230–400 and RP-HPLC. RP-HPLC was performed using a UHPLC Shimadzu. All the solvents were used after distillation. The melting point of the isolated compound was measured from Equiptronics (EQ-730) melting point apparatus. The TLC was analysed on a silica gel pre-coated aluminium-based plate, visualised with UV light, iodine vapour, or H_2SO_4 in MeOH staining solution wherever needed.

Experimental section for Isolation and Synthesis

Plant material

The leaves of *G. wynaadensis* Bedd. were collected from wild plants growing hilly forest region of Wayanad district, Kerala, namely Peria forest, Chembra hills, and Thamarasserey garden (Western Ghats) during the non-flowering season. The plant identification was done by Taxonomist from M.S. Swaminathan Research Foundation

© 2023 Wiley-VHCA AG, Zurich, Switzerland

(MSSRF) at Community Agrobiodiversity Center, Puthoorvayal, Kalpetta, Wayanad, Kerala, India. The herbarium voucher specimen (MSSH WAYANAD No. 0462) was deposited at MSSRF Herbarium.

Extraction and isolation

The powder of dried *G. wynaadensis* leaves (2.5 Kg) was soaked in solvents in order of increasing polarity in the aspirator and collected as six separate extracts, as described in our previous article.[18] Following the bio-guided fractionation results, the most active extract – Ethyl Acetate extract (2.5 g) was subjected to column chromatography (CC) using silica gel, and eluted via gradient method using hexane-ethyl acetate solvent system to yield fractions GWEAex1 (90:10), GWEAex2 (80:20), GWEAex3 (70:30), GWEAex4 (60:40), GWEAex5 (50:50), and GWEAex6 (40:60). Fraction GWEAex3 (70:30) (89 mg), yielded two UV active, charring active spots. These were further separated by column chromatography using 230–400 mesh silica gel to yield goniothalamin (**1**) (36 mg) and (+)-goniothalamin oxide (**2**) (40 mg). Fraction GWEx4 (60:40) (388 mg) yielded two UV active, charring active spots, which were found to be goniodiol-7-monoaccetate (**3**) (180 mg) and goniodiol-8-monoacetate (**4**) (165 mg). Further, more polar fraction GWEAex5 (50:50) (90 mg) yielded goniodiol (**5**) (68 mg) using 100–200 mesh size silica gel CC. Fraction GWEAex6 (40:60) (300 mg) yielded (+)-8-epi-9-deoxygoniopypyrone (**6**) and (−)-8-epi-9-deoxygoniopypyrone (**7**), which were further separated using the reverse phase-high performance liquid chromatography (RP-HPLC). The linear gradient of methanol with water was used as the mobile phase in HPLC; compounds **6** and **7** were eluted at 40% of methanol with retention time at 16.54 min. and 17.62 min., respectively.

The methanol extract (2 g) was chromatographed on silica gel CC, and eluted via gradient method using hexane-ethyl acetate solvent system to yield fraction GWMex1 (90:10), GWMex2 (80:20), GWMex3 (70:30), GWMex4 (60:40), GWMex5 (50:50), etc. Out of these fractions, GWMex3 (70:30) fraction has an UV active as well as charring active spot, which was further separated by a flash column chromatography using 230–400 mesh silica gel yielded 8-methoxygoniodiol (**8**) (20 mg).

Acetylation of compounds 3 and 4

Compound **3/4** (0.5 mmol) was taken in a 25 ml round bottom flask. To this, excess acetic anhydride (5 mmol) was added. The reaction mixture was allowed to stir at room temperature. To this reaction mixture, pyridine (1 mmol) was added. The reaction mixture was allowed to stir for 4 h and was monitored by TLC. On completion of the reaction, pyridine in the reaction mixture was quenched with saturated copper sulfate solution. It was further extracted with water and ethyl acetate (3×10 mL). The organic layer was separated, dried over sodium sulfate and evaporated under a vacuum. Pure compound **9** was separated by flash column chromatography.

Spectroscopic data

Goniothalamin (1)

Solid, m.p. = 80–82 °C; [α]0*pt*25D −70 (*c* = 0.0017, $CHCl_3$); IR (cm^{-1}): ν_{max} 1731, 1497, 1457, 1268. ^{1}H-NMR ($CDCl_3$, 400 MHz) δ 7.41–7.26 (5H, m, H-10–H-14), 6.93 (1H, dt, *J* = 9.6, 4.4, H-4), 6.73 (1H, dd, *J* = 16.0, 0.8, H-8), 6.28 (1H, dd, *J* = 16, 6.4, H-7), 6.09 (1H, dd, *J* = 8.2, 4, H-3), 5.11 (1H, m, H-6), 2.55 (2H, m, H-5). ^{13}C-NMR ($CDCl_3$, 100 MHz) δ 162.9 (C-2), 143.6 (C-4), 134.8 (C-9), 132.2 (C-8), 127.7 (C-11), 127.7 (C-13), 127.4 (C-12), 125.7 (C-10), 125.7 (C-14), 124.7 (C-7), 120.7 (C-3), 77.0 (C-6), 28.9 (C-5). ESI-MS: *m/z* 201.20 $[M+H]^+$ calc. for $C_{13}H_{13}O_2$, 201.08.

(+)-Goniothalamin oxide (2)

Viscous compound; [α]0*pt*25D +28.62 (*c* = 0.0025, $CHCl_3$); IR (cm^{-1}): ν_{max} 1725, 1457, 1243, 1156, 1082. ^{1}H-NMR ($CDCl_3$, 400 MHz) δ 7.38–7.26 (5H, m, H-10–H-14), 6.94 (1H, dddd, *J* = 9.8, 3.6, H-4), 6.07 (1H, td, *J* = 9.6, 1.6, H-3), 4.45 (1H, td, *J* = 9.6, 5.6, H-6), 3.90 (1H, d, *J* = 2.0, H-8), 3.27 (1H, dd, *J* = 5.7, 2, H-7), 2.59 (2H, m, H-5) and ^{13}C-NMR ($CDCl_3$, 100 MHz) δ 162.8 (C-2), 144.3 (C-4), 135.6 (C-9), 128.7 (C-12), 128.6 (C-11), 128.6 (C-13), 125.7 (C-10), 125.7 (C-14), 121.5 (C-3), 77.1 (C-6), 61.5 (C-7), 57.2 (C-8), 25.9 (C-5). HR-ESI-MS: *m/z* 217.0862 $[M+H]^+$ calc. for $C_{13}H_{13}O_3$, 217.0865.

Goniodiol-7-monoacetate (3)

White crystals, m.p. = 146–148 °C; [α]0*pt*25D +16.4 (*c* = 0.025, $CHCl_3$); IR (cm^{-1}) ν_{max}: 3417, 1731, 1494, 1455, 1266, 1228. ^{1}H-NMR ($CDCl_3$, 500 MHz) δ 7.41–7.29 (5H, m, H-10–H-14), 6.89 (1H, ddd, *J* = 10, 5.7, 3, H-4), 6.03 (1H, ddd, *J* = 10, 2.5,1.5, 1, H-3), 5.13 (1H, d, *J* = 2.5, H-7), 5.11 (1H, dd, *J* = 8.5, 1.5, H-8), 5.07 (1H, ddd, *J* = 10.5, 4.5, 1.5, H-6), 2.35 (1H, ddd, *J* = 16.5, 10.5, 2.5 H-5), 2.31 (1H, dddd, *J* = 16.7, 10.5, 3.5, 1, H-5), 1.82, (3H, s), and ^{13}C-NMR ($CDCl_3$, 125 MHz) δ 169.7 (7-OC=O), 163.6 (C-2), 145.1 (C-4), 140.4 (C-9), 128.4 (C-11; C-13; C12), 126.8 (C-10; C-14), 121.1 (C-3), 75.3 (C-7), 75.0 (C-6), 71.1 (C-8), 26.2 (C-5), 20.39 (7-$OCOCH_3$). HR-ESI-MS: *m/z* 277.1069 $[M+H]^+$ calc. for $C_{15}H_{17}O_5$, 277.1076.

Goniodiol-8-monoacetate (4)

White amorphous powder, m.p. = 112–114 °C; [α]0*pt*25D +3.92 (*c* = 0.026, $CHCl_3$); IR (cm^{-1}) ν_{max}: 3450, 1741, 1491, 1485, 1243 cm^{-1}; ^{1}H-NMR ($CDCl_3$, 500 MHz) δ 7.40–7.31 (5H, m, H-10–H-14), 6.92 (1H, ddd, *J* = 9.5, 5.5, 2, H-4), 6.01 (1H, ddd, *J* = 9.5, 4, 1, H-3), 5.88 (1H, d, *J* = 7.5, H-8), 4.65 (1H, ddd, *J* = 12.5, 6, 2.5, 1, H-6), 3.90 (1H, dd, *J* = 7.5, 2, H-7), 2.78 (1H, ddt, *J* = 18, 12.5, 5.5, 2.5, H-5), 2.41(1H, br. s), 2.25 (1H, ddd, *J* = 18, 6, 4.5, 1, H-5), 2.06 (3H, s, 8-$OCOCH_3$) and ^{13}C-NMR ($CDCl_3$, 125 MHz) δ 169.6 (8-OC=O), 163.2 (C-2), 145.2 (C-4), 137.1 (C-9), 128.6 (C-11), 128.6 (C-13), 128.6 (C-12), 127.5 (C-10), 127.5 (C-14), 121.0 (C-3), 76.1 (C-8), 74.6 (C-6), 74.0 (C-7), 26.0 (C-5), 21.09. HR-ESI-MS: *m/z* 277.1071 $[M+H]^+$ calc. for $C_{15}H_{17}O_5$, 277.1076.

Goniodiol (5)

Viscous oil; [α]0*pt*25D +38.70 (*c* = 0.0046, $CHCl_3$); IR (cm^{-1}) ν_{max}: 3386, 1696, 1494, 1454, 1254 cm^{-1}; ^{1}H-NMR ($CDCl_3$, 500 MHz) δ 7.41–7.30 (5H, m, H-10–H-14), 6.91 (1H, dddd; *J* = 9.5, 6, 4, 2, H-4), 5.97 (1H, dddd, *J* = 9.75, 3, 2, H-3), 4.93 (1H, d, *J* = 7.5, H-8), 4.79 (1H, dddd, *J* = 12.5, 3.5, 2.5, H-6), 3.70 (1H, d, *J* = 6.5 Hz, H-7), 2.98 (1H, br, s, 8-OH), 2.77 (1H, ddt; *J* = 18.5, 12.5, 2.5, H-5), 2.49 (1H, br. s, 7- OH), 2.17 (1H, dddd, *J* = 18, 6.0, 4, 1, H-5) and ^{13}C-NMR ($CDCl_3$, 125 MHz) δ 163.7 (C-2), 146.1 (C-4), 140.0 (C-9), 128.7 (C-11), 128.7 (C-13), 128.2 (C-12), 126.5 (C-10), 126.5 (C-14), 120.5 (C-3), 76.7 (C-6), 75.0 (C-7), 73.6 (C-8), 26.0 (C-5). HR-ESI-MS: *m/z* 235.0966 $[M+H]^+$ calc. for $C_{13}H_{15}O_4$, 235.0970.

(+)-8-Epi-9-deoxygoniopypyrone (6)

White solid, m.p. = 130–132 °C; [α]0*pt*25D −30 (*c* = 0.0015, $CHCl_3$); IR (cm^{-1}) ν_{max}: 3397, 1737, 1497, 1455, 1266; ^{1}H-NMR ($CDCl_3$, 400 MHz) δ 7.41–7.36 (5H, m, H-11–H-15), 4.93 (1H, br. s, H-1), 4.46 (1H, br. s,

© 2023 Wiley-VHCA AG, Zurich, Switzerland

H-5), 4.43 (1H, br. s, H-7), 3.59 (1H, d, $J=8.5$, H-8), 2.99 (1H, d, $J=24$, H-4), 2.88 (1H, dd, $J=24.5$, H-4), 2.52 (1H, br. s, 8-OH), 2.23 (2H, s, H-9), ^{13}C-NMR ($CDCl_3$, 100 MHz) δ 168.9 (C-3), 137.8 (C-10), 128.7 (C-12), 128.7 (C-14), 128.6 (C-13), 127.3 (C-11), 127.3 (C-15), 76.7 (C-1), 74.3 (C-7), 72.6 (C-8), 65.8 (C-5), 36.5 (C-4), 29.8 (C-9). HR-ESI-MS: *m/z* 235.0965 $[M+H]^+$, *m/z* 257.0782 $[M+Na]^+$ calc. for $C_{13}H_{15}O_4$, 235.0970.

(−)-8-Epi-9-deoxygoniopypyrone (7)

Viscous oil; [α]0*pt*25D +16.31 ($c=0.0019$, $CHCl_3$); IR (cm^{-1}) ν_{max}: 3406, 1734, 1494, 1454, 1250 cm^{-1}, ^{1}H-NMR ($CDCl_3$, 500 MHz) δ 7.42–7.34 (5H, m, H-11–H-15), 4.95 (1H, m, H-1), 4.48 (1H, m, H-5), 4.43 (1H, d, $J=9.5$, H-7), 3.64 (1H, dd, $J=9.5$, 2.5, H-8), 3.00 (1H, d, $J=19.7$, H-4), 2.88 (1H, dd, $J=19.25$, 4.8, H-4), 2.24 (2H, m, H-9a and b), ^{13}C-NMR ($CDCl_3$, 125 MHz) δ 168.8 (C-3), 137.7 (C-10), 128.7 (C-12), 128.7 (C-14), 128.6 (C-13), 127.3 (C-11), 127.3 (C-15), 76.6 (C-1), 74.4 (C-7), 72.6 (C-8), 65.8 (C-5), 36.6 (C-4), 29.9 (C-9). HR-ESI-MS: *m/z* 235.0966 $[M+H]^+$, *m/z* 257.0784 $[M+Na]^+$ calc. for $C_{13}H_{15}O_4$, 235.0970.

8-Methoxygoniodiol (8)

Viscous oil, IR (KBr) ν_{max}: 3450, 1741, 1496, 1485, 1243 cm^{-1}; ^{1}H-NMR ($CDCl_3$, 500 MHz) δ 7.40–7.32 (5H, m, H-10–H-14), 6.91(1H, ddd, $J=$ 9.5, 6, 2.5, H-4), 6.00 (1H, ddd, $J=9.5$, 3, 0.5, H-3), 4.35, (1H, d, $J=$ 7.5, H-8), 4.33 (1H, td, $J=9.5$, 5.5, 4, H-6), 4.15 (1H, t, $J=6$, 5.5, H-7), 3.24 (3H, s, 8-OCH_3), 2.65 (1H, ddt, $J=18.5$, 11.5, 5.5, 2.5, H5), 2.41 (1H, ddd, $J=18.5$, 6, 4, H-5) and ^{13}C-NMR ($CDCl_3$, 125 MHz) δ 163.7 (C-2), 145.6 (C-4), 136.9 (C-9), 128.5 (C-11), 128.5 (C-13), 128.4 (C-12), 127.9 (C-10), 127.9 (C-14), 120.9 (C-3), 82.6 (C-8), 77.4 (C-6), 74.4 (C-7), 56.8, 24.4 (C-2). HR-ESI-MS: *m/z* 249.1118 $[M+H]^+$ calc. for $C_{14}H_{17}O_4$, 249.1127.

Goniodiol diacetate (9)

White solid, yield: 90%; m.p.=155–157 °C; [α]0*pt*25D +110.41 ($c=$ 0.0017, $CHCl_3$); IR (cm^{-1}) ν_{max}: 1731, 1494, 1455, 1266, 1228 cm^{-1}; ^{1}H-NMR (500 MHz, $CDCl_3$): δ 7.38–7.28 (m, 5H, H-10–H-14), 6.85 (1H, dddd, $J=9.75$, 5.5, H-4), 6.03 (2H, m, H-3 and H-8), 5.35 (1H, dd, $J=$ 8.5, 2.5, H-7), 4.76 (1H, dddd, $J=10.75$, 5, H-6), 2.41-2.31 (2H, m, H-5), 2.08 (3H, s), 1.82 (3H, s); ^{13}C-NMR ($CDCl_3$, 125 MHz) δ 169.7 (8-C=O), 168.9 (7-C=O), 162.8 (C-2), 144.1 (C-4), 136.4 (C-9), 128.6 (C-12), 128.4 (C-11), 128.4 (C-13), 127.4 (C-10), 127.4 (C-14), 121.4 (C-3), 74.6 (C-8), 73.5 (C-7), 72.3 (C-6), 26.0 (C-5), 20.9, 20.2. HR-ESI-MS: *m/z* 319.1173 $[M+H]^+$ calc. for $C_{17}H_{19}O_6$, 319.1182.

Experimental section for Anticancer activity

Cell culture procedure

The cell lines, breast (MDA-MB-231), prostate (PC3), colon (HCT-15), ovarian (SKOV3) and human embryonic kidney cell lines (HEK-293) were procured from National Center for Cell Science, Pune, India. The cells were cultured in media such as Dulbecco's modified eagle's medium (DMEM), Roswell Park memorial institute (RPMI-1640) supplemented with 10% (V/V) Fetal bovine serum (FBS), 100 units/ mL of penicillin, and streptomycin. All cell lines were cultured and incubated at 37 °C humidified atmosphere with 5% CO_2.

MTT assay procedure

The natural isolated compound's cytotoxicity activity was evaluated by MTT assay on human breast cancer cell lines (MDA-MB-231), human prostate cancer cell lines (PC3), human ovarian cancer cell lines (SKOV3), human colon cancer cell lines (HCT-15) and human embryonic kidney cell lines (HEK-293). Cells (1×10^4 cells/well −100 μL each) were seeded in 96 well micro-culture plates and were supplemented with 10% FBS, 1% penicillin-streptomycin incubated at 37 °C in 5% CO_2 humidified incubator for 24 h. After cells attained morphology, the test compounds at different concentrations were added to each well for 24 h incubation. Vincristine was used as a positive control. At the end of the exposure, 20 μL freshly prepared MTT reagent (3-(4,5-dimethylthiazol-2-yl)-2,5-diphenyltetrazolium bromide) in 5 mg/mL in phosphate-buffered saline (PBS) was added to each well. The supernatant was discarded from each well and replaced with DMSO to dissolve the Formazan crystals. The absorbance was recorded for 570 nm wavelength at the spectrophotometer/ microplate reader. The equation for calculating cell viability was: % Cell Viability = $(OD_{Sample}/OD_{Control})\times100$, after which IC_{50} was calculated, which is the average triplicate readings.

Cell cycle analysis procedure

The effect of the compound goniodiol-7-monoacetate (**3**) on the DNA content of the cell cycle progression was assessed on MDA-MB-231 cancer cells. MDA-MB-231cells (2×10^5) were plated in a −6 well plate with complete media (serum-free) and allowed to adhere to overnight incubation. After 24 h, media was replaced with and without compounds vincristine (VIN) and goniodiol-7-monoacetate (**3**) (Experiment Code – **HBT-96 A**) at indicated concentrations and incubated for 24 h. The cells were washed thrice with PBS, fixed with ice-cold PBS in 70% ethanol and stored at −20 °C for 30 min. After fixation, these cells were incubated with RNase (0.1 mg/ml) at 37 °C for 30 min, stained with Propidium iodide (50 μg/mL) for 30 min ice-cold dark conditions and measured the DNA content by using BD FACSVerse flow cytometer.

Annexin V/PI staining assay procedure

Annexin V/PI assay was carried out using the Annexin V FITC detection kit (Sigma Aldrich APOAF 20TST). Briefly, MDA-MB-231 cells were plated in 6 well plates at a density of 2×10^5 cell/well and allowed to attach overnight, followed by treatment with indicated concentrations of vincristine and goniodiol-7-monoacetate (**3**) (HBT-96 A) for 24 h. After 24 h, media was discarded, gently trypsinised the cells and resuspended the cells in 1X Annexin binding buffer at a concentration of 1×10^6 cell/mL. The cells were incubated with 5 μL of Annexin-V-FITC and 10 μL of Propidium iodide for 10 min at room temperature and protected from the light. The staining buffer was aspirated after centrifugation at 4 °C for 5 min and cells were resuspended in 100 μL. Afterwards, analysis was carried out using a flow cytometer (BD FACSVerse, Becton-Dickinson, USA).

Experimental section for Molecular modelling methodology

Protein preparation for molecular modelling analysis

Crystal structures of Tubulin were retrieved from the protein databank (PDB). The PDB code, 5FNV, was employed in the investigations, and the three-dimensional structures of 5FNV were analysed using the Schrodinger software platform Maestro Version 12.0.012. The residue around 4 Å distance to the Cysteine in

© 2023 Wiley-VHCA AG, Zurich, Switzerland

structure was identified using Maestro Version 12.0.012. Using PROPKA at pH 7, sample water orientations were produced, hydrogen atoms were provided, and water in the protein with less than three hydrogen bonds to non-waters was removed. Using the OPLS3e force field, the main protein-ligand complex's restrained minimisation was accomplished. Finally, the protein was saved in PDB format for docking.

Preparation of ligand

The three-dimensional structures of isolated compounds and the Pironetin molecule were drawn in a 2D sketcher of Schrodinger and saved with an individual name. The calculations for ligand preparation are set up using the LigPrep panel. LigPrep, which creates many output structures for each input structure by creating various protonation states, configuration, tautomers, and ring conformations, was used to create stable low-energy 3D structures.

Covalent docking of isolated molecules into tubulin complex

The Pironetin molecule and isolated compounds were used in the covalent docking analysis of α-tubulin in the Maestro Version 12.0.012 platform of the Schrodinger programme to determine the binding energy (Kcal mol^{-1}). The receptor grid was defined in the coordinate region ranging from 10 to 12 Å by defining the amino acid residue at the active site of α-tubulin, that is, Cys-316 at chain C under default settings. The maximum number of poses to retain for further refinement was kept default in the covalent docking panel, which is 200.

Computational study of the reaction between cysteine thiol and isolated molecules

Density functional theory (DFT) calculations were performed using the Maestro Material Science 3.4.012 platform of the Schrodinger programme to evaluate the Gibbs free energy change (△G) values for hypothetical reactions involving Cysteine and isolated molecules and pironetin. Molecules were optimised using B3LYP-D3 on the Jaguar platform (version: 10.2, Schrodinger release 2019-2) with a 6-31G** basis set and polarisation function on all atoms. The accuracy level was set to ultrafine with default convergence criteria, and the solvent model was none and maximum iteration steps of 100 with a switch to analytical integrals near convergence. Gibbs free energies are stated in (kcal/mol) assuming standard condition (T = 298.15 K and p = 1.0 bar).

Acknowledgements

The author HH would like to acknowledge DST-SERB, New Delhi, for partial financial assistance with grant SB/S1/OC-76/2013. Authors AS, DT and HH acknowledge the taxonomical help provided by M.S. Swaminathan Research Foundation (MSSRF) at Community Agrobiodiversity Center, Puthoorvayal, Kalpetta, Wayanad, Kerala, India. Authors DT, AS and HH express their sincere acknowledgement to Prof. Halmathur Sampath Kumar-Vaccine Immunology Laboratory, CSIR-Indian Institute of Chemical Technology, Hyderabad, for insightful help in anticancer studies. The authors would like to acknowledge NCBS, Bangalore, for recording HR-ESI-MS. The authors thank the Hon'ble Vice-Chancellor, Central University of Karnataka, Kalaburagi. Doddabasappa Talimarada thanks the Central University of Karnataka for a research fellowship.

Conflict of Interests

The authors declare no conflict of interest.

Data Availability Statement

The data that support the findings of this study are available in the supplementary material of this article.

Keywords: anticancer activity · DFT · goniodiol-7-monoacetate · *Goniothalamus wynaadensis* · molecular modelling

[1] C. Wiart, *Evid.-Based Complement. Altern. Med.* **2007**, *4*, 299–311.
[2] M. S. Aslam, *Recent Adv. Biol. Med.* **2016**, *4*.
[3] G. C. L. Ee, H. L. Lee, S. H. Goh, *Nat. Prod. Lett.* **1999**, *13*, 137–142.
[4] C.-J. Chang, Y.-M. Liu, A. Alkofahi, J. K. Rupprecht, D. L. Smith, *Experientia.* **1988**, *44*, 83–85.
[5] M. A. Seyed, I. Jantan, S. Nasir, A. Bukhari, Natural Bioactives in Cancer Treatment and Prevention, **2014**.
[6] M. A. Blázquez, A. Bermejo, M. C. Zafra-Polo, D. Cortes, *Phytochem. Anal.* **1999**, *10*, 161–170.
[7] M. T. Davies-Coleman, J. Galambos, L. Hough, C. E. James, R. Khan, K. Krohn, M. Lounasmaa, D. E. A. Rivett, *Springer Science & Business Media* **2012**.
[8] A. de Fatima, L. Modolo, L. Conegero, R. Pilli, C. Ferreira, L. Kohn, J. de Carvalho, *Curr. Med. Chem.* **2006**, *13*, 3371–3384.
[9] C. Wiart, *Evid.-Based Complement. Altern. Med.* **2007**, *4*, 299–311.
[10] K. Jewers, J. B. Davis, J. Dougan, A. H. Manchanda, G. Blunden, A. Kyi, S. Wetchapinan, *Phytochemistry* **1972**, *11*, 2025–2030.
[11] M. Al-Qubaisi, R. Rosli, T. Subramani, A. R. Omar, S. K. Yeap, A. M. Ali, N. B. Alitheen, *Nat. Prod. Res.* **2013**, *27*, 2216–8.
[12] P. J. Clarke, P. J. Pauling, *J. Chem. Soc.-Perkin Trans.* **1975**, *2*, 368–370.
[13] R. Pei, T. Kim, V. Bihud, K. Mohamad, K. H. Leong, J. Mohamad, F. Ahmad, H. Hazni, N. Kasim, S. Nadiah, A. Halim, K. Awang, *Molecules* **2013**, *18(1)*, 128–139.
[14] A. M. Alabsi, R. Ali, A. M. Ali, S. A. Al-Dubai, H. Harun, N. H. Abu Kasim, A. Alsalahi, *Asian Pacific J. Cancer Prev.* **2012**, *13*, 5131–5136.
[15] C-C. Chiu, P-L. Liu, K-J. Huang, H-M. Wang, K-F. Chang, C-K. Chou, F-R. Chang, I-W. Chong, K. Fang, J-S. Chen, H-W. Chang, Y-C. Wu, *J. Agric. Food Chem.* **2011**, *27;59(8)*, 4288–93.
[16] R. C. Barcelos, K. J. Pelizzaro-Rocha, J. C. Pastre, M. P. Dias, C. V. Ferreira-Halder, R. A. Pilli, *Eur. J. Med. Chem.* **2014**, *87*, 745–758.
[17] M. D. Ajithabai, B. Rameshkumar, G. Jayakumar, L. Varma, M. S. Nair, *Indian J. Chem. Sect. B – Org. Med. Chem.* **2011**, *50*, 1786–1793.
[18] A. Sharma, P. Sharma, S. Singh, T. B. Karegoudar, H. Holla, *Eur. J. Integr. Med.* **2019**, *32*, 101000.
[19] J. R. Hlubucek, A. Robertson, *Aust. J. Chem.* **1967**, *20*, 2199–2206.
[20] K. Jewers, J. B. Davis, J. Dougan, A. H. Manchanda, G. Blunden, A. Kyi, S. Wetchapinan, *Phytochem.* **1972**, *11*, 2025–2030.
[21] T. W. Sam, C. Sew-Yeu, S. Matsjeh, E. K. Gan, D. Razak, A. L. Mohamed, *Tetrahedron Lett.* **1987**, *28*, 2541–2544.
[22] C. H. Chuah, G. C. L. Ee, C. Wei, *Aust. J. Chem.* **1995**, *48*, 199–205.
[23] Y. C. Wu, C. Y. Duh, F. R. Chang, G. Y. Chang, S. K. Wang, J. J. Chang, D. R. McPhail, A. T. McPhail, K. H. Lee, *J. Nat. Prod.* **1991**, *54*, 1077–1081.
[24] S. K. Talapatra, D. Basu, T. Deb, S. Goswami, B. Talapatra, *Indian J. Chem. B.* **1985**, *24*, 29–34.
[25] Y. C. Wu, F. R. Chang, C. Y. Duh, S. K. Wang, T. S. Wu, *Phytochemistry* **1992**, *31*, 2851–2853.
[26] X. P. Fang, J. E. Anderson, C. J. Chang, J. L. McLaughlin, P. E. Fanwick, *J. Nat. Prod.* **1991**, *54*, 1034–1043.
[27] J. R. Liou, T. Y. Wu, T. D. Thang, T. L. Hwang, C. C. Wu, Y. Bin Cheng, M. Y. Chiang, Y. H. Lan, M. El-Shazly, S. L. Wu, L. Beerhues, S. S. Yuan, M. F. Hou, S. L. Chen, F. R. Chang, Y. C. Wu, *J. Nat. Prod.* **2014**, *77*, 2626–2632.

© 2023 Wiley-VHCA AG, Zurich, Switzerland

[28] T. Yoshida, S. Yamauchi, R. Tago, M. Maruyama, K. Akiyama, T. Sugahara, T. Kishda, Y. Koba, *Biosi. Biotechnol. Biochem.* **2008**, *72*, 2342–2352.
[29] J. P. Surivet, J. M. Vatèle, *Tetrahedron Lett.* **1997**, *38*, 819–820.
[30] Y. H. Lan, F. R. Chang, C. C. Liaw, C. C. Wu, M. Y. Chiang, Y. C. Wu, *Planta Med.* **2005**, *71*, 153–159.
[31] B. H. Tai, V. T. Huyen, T. T. Huong, N. X. Nhiem, E. M. Choi, J. A. Kim, P. Q. Long, N. M. Cuong, Y. H. Kim, *Chem. Pharm. Bull.* **2010**, *58*, 521–525.
[32] M. Kondoh, T. Usui, S. Kobayashi, K. Tsuchiya, K. Nishikawa, T. Nishikiori, T. Mayumi, H. Osad, *Cancer Lett.* **1998**, *126*, 29–32.
[33] S. Torijano-Gutierrez, C. Vilanova, S. Dıaz-Oltra, J. Murga, E. Falomir, M. Carda, M. Redondo-Horcajo, J. Fernando Dıaz, I. Barasoain, J. A. Marco, *Arch. Pharm. Chem. Life Sci.* **2015**, *348*, 541–547.
[34] J. Yang, Y. Wang, T. Wang, J. Jiang, C. H. Botting, H. Liu, Q. Chen, J. Yang, J. H. Naismith, X. Zhu, L. Chen, *Nat. Commun.* **2016**, *7*, 1–9.
[35] R. Fraczkiewicz, W. Braun, *J. Comput. Chem.* **1998**, *19*, 319–333.
[36] S. K. Coulup, G.I. Georg, *Chem. Lett.* **2019**, *29*, 1865–1873.
[37] J. Yang, Y. Wang, T. Wang, J. Jiang, C. H. Botting, H. Liu, Q. Chen, J. Yang, J. H. Naismith, X. Zhu, *Nat. Commun.* **2016**, *7*, 1–9.

Manuscript received: March 13, 2023
Accepted manuscript online: July 21, 2023
Version of record online: ■■, ■■

© 2023 Wiley-VHCA AG, Zurich, Switzerland